Mon. Not. R. Astron. Soc. **000**, 1–9 (2008) Printed 6 April 2008 (MN LATEX style file v2.2)

The probability distribution of cluster formation times and implied Einstein Radii

Sharon Sadeh[1⋆], Yoel Rephaeli[1,2]
[1] *School of Physics and Astronomy, Tel Aviv University, Tel Aviv, 69978, Israel*
[2] *Center for Astrophysics and Space Sciences, University of California, San Diego, La Jolla, CA 92093-0424*

6 April 2008

ABSTRACT

We provide a quantitative assessment of the probability distribution function of the concentration parameter of galaxy clusters. We do so by using the probability distribution function of halo formation times, calculated by means of the excursion set formalism, and a formation redshift-concentration scaling derived from results of N-body simulations. Our results suggest that the observed high concentrations of several clusters are quite unlikely in the standard ΛCDM cosmological model, but that due to various inherent uncertainties, the statistical range of the predicted distribution may be significantly wider than commonly acknowledged. In addition, the probability distribution function of the Einstein radius of A1689 is evaluated, confirming that the observed value of $\sim 45" \pm 5"$ is very improbable in the currently favoured cosmological model. If, however, a variance of $\sim 20\%$ in the theoretically predicted value of the virial radius is assumed, then the discrepancy is much weaker. The measurement of similarly large Einstein radii in several other clusters would pose a difficulty to the standard model. If so, earlier formation of the large scale structure would be required, in accord with predictions of some quintessence models. We have indeed verified that in a viable early dark energy model large Einstein radii are predicted in as many as a few tens of high-mass clusters.

Key words: cosmology:large-scale structure of Universe – gravitational lensing – galaxies:clusters:general

1 INTRODUCTION

The formation of galaxies and their systems ('haloes') is known to be more intricate than its simplified rendering in the context of spherical collapse models. The process is characterised by gradual growth of the system mass and evolution of its morphological properties through multiple merging events, evidence for which comes from observations and hydrodynamical simulations. In clusters, mergers affect also the evolution of intracluster (IC) gas density and temperature and their spatial profiles. On the theoretical side, studies of halo mergers and related issues began with the works of Bond et al. (1991) and Lacey & Cole (1993), who developed the theory of *excursion sets* in the context of structure formation. This approach was originally devised by Bond et al. in order to address the "cloud-in-cloud" problem, who showed that the Press & Schechter (1974) mass function, including the "fudge factor" of 2, could be derived under certain assumptions. They also used their formalism to derive expressions for merger probabilities. Lacey & Cole (hereafter LC) used the excursion set formalism (ESF) to extract such related quantities as halo merger rates, halo survival times, and halo formation times.

The NFW concentration parameter (Navarro, Frenk, & White 1995), which characterises dark matter (DM) distribution in a halo is known from N-body simulations to be correlated with its formation time (e.g. Jing 2000; Bullock et al. 2001; Zhao et al. 2003) due to the fact that haloes which form earlier are likely to have more condensed cores, reflecting the higher background density of the universe. We use this inferred correlation, and the probability distribution function (PDF)

⋆ E-mail: shrs@post.tau.ac.il

of halo formation times, to construct PDFs of halo concentrations. This provides a convenient framework for a comparison of theoretically predicted values of the concentration parameter to observational results. Our calculations of the formation time and concentration parameter PDFs are carried out in a standard ΛCDM cosmology, adopting the set of cosmological parameters,$(\Omega_m, \Omega_\Lambda, h, n, \sigma_8) = (0.3 \pm 0.021, 0.7 \pm 0.021, 0.687 \pm 0.018, 0.953 \pm 0.016, 0.827^{+0.026}_{-0.025})$, extracted from the 3-year WMAP+WL data (Spergel et al. 2007). These parameters are selected for the sake of consistency with results obtained in other works, including calculations of the PDF of Einstein radii. Specifically, we show that the observed high Einstein radius in the lensing cluster A1689, whose value is roughly in the range $40" - 50"$ (e.g., Broadhurst & Barkanna 2008), is very improbable in the standard ΛCDM cosmology, but much more probable in a cosmological model characterised by an early component of dark energy, provided that its virial radius is larger (within a plausible range of variance) than what is predicted in the simple spherical collapse scenario.

This paper is arranged as follows: In §2 we briefly detail the derivation of the PDFs of halo formation time and concentration parameter; results are provided in §3. The case of the lensing cluster A1689 is explored in §4, followed by a discussion, §5.

2 METHOD

2.1 PDF of formation times

In the LC formalism the cumulative distribution function (CDF) of halo formation times, which describes the probability that a halo of mass M_2 had a parent with mass in the range $[fM_2 < M_1 < M_2]$ at redshift z_1, with f denoting the fraction of mass assembled through mergers by redshift z_1 is,

$$P(M_1 > fM_2, z_1 | M_2, z_2) = \int_{S_2}^{S_h} \frac{M(S_2)}{M(S_1)} f_{S_1}(S_1, \delta_{c_1} | S_2, \delta_{c_2})\, dS_1. \quad (1)$$

Here $S \equiv \sigma^2$ and δ_c denote the mass variance and critical density for spherical collapse, respectively, with δ_c extrapolated to $z = 0$, and $f_{S_1}(S_1, \delta_{c_1} | S_2, \delta_{c_2})$ is the conditional probability that a halo with mass M_2 at time t_2 had a progenitor of mass M_1 at time t_1. Put in the language of the ESF, this is the probability that a random walk trajectory which reached the δ_{c_2} barrier at mass scale M_2 had traversed for the first time the δ_{c_1} barrier at mass scale M_1. This probability is the key result from the ESF which is used to determine the halo mass function and quantities related to its hierarchical evolution, such as the PDF of formation times. For primordial Gaussian density fields,

$$f_{S_1}(S_1, \delta_{c_1} | S_2, \delta_{c_2}) dS_1 = \frac{(\delta_{c_1} - \delta_{c_2})}{(2\pi)^{1/2}(S_1 - S_2)^{3/2}} \exp\left[-\frac{(\delta_{c_1} - \delta_{c_2})^2}{2(S_1 - S_2)}\right] dS_1. \quad (2)$$

This analytical result derived from the ESF is an outcome of the fact that smoothed Gaussian fields still obey a Gaussian distribution, and inherently includes the "fudge factor" of 2 which Press & Schechter have "artificially" introduced into their mass function so as to ensure that all the mass is included in haloes. The PDF of halo formation times can be now obtained by differentiating equation (1) with respect to the redshift:

$$p_z(z) = -\frac{\partial P(M_1 > fM_2, z1 | M_2, z_2)}{\partial z}. \quad (3)$$

The definition of halo formation time is somewhat arbitrary; haloes are commonly considered to have formed when a fraction f of their total mass was assembled, usually with either $f = 0.5$ or $f = 0.75$. It is important to make the distinction between the observation and formation times: The former corresponds to the redshift at which the halo is observed to be; the formation redshift is distributed in the range (z_{obs}, ∞), and its PDF must satisfy

$$\int_{z_{obs}}^{\infty} p_z(z)\, dz = 1. \quad (4)$$

2.2 PDF of halo concentrations

The concentration parameter is defined as $c_v = R_v/R_s$, where R_v is the virial radius of the halo and R_s is a characteristic inner radius, which roughly marks the transition radius from a $\sim 1/r$ to $\sim 1/r^3$ behaviour of the NFW density profile (Navarro, Frenk, & White 1995). Results of N-body simulations suggest that haloes formed at higher redshifts tend to be associated with higher concentration parameters. This has been explained as an outcome of the formation of higher density cores when the background density was higher. This association directly implies also a correlation between the concentration parameter and formation time, evidence for which has been seen in N-body simulations of DM haloes (e.g. Zhao et al. 2003, Wechsler et al. 2002).

An analytic expression describing the correlation between the concentration parameter and formation time can be used in order to derive a PDF of halo concentrations, yielding the probability of finding a given concentration parameter for a given

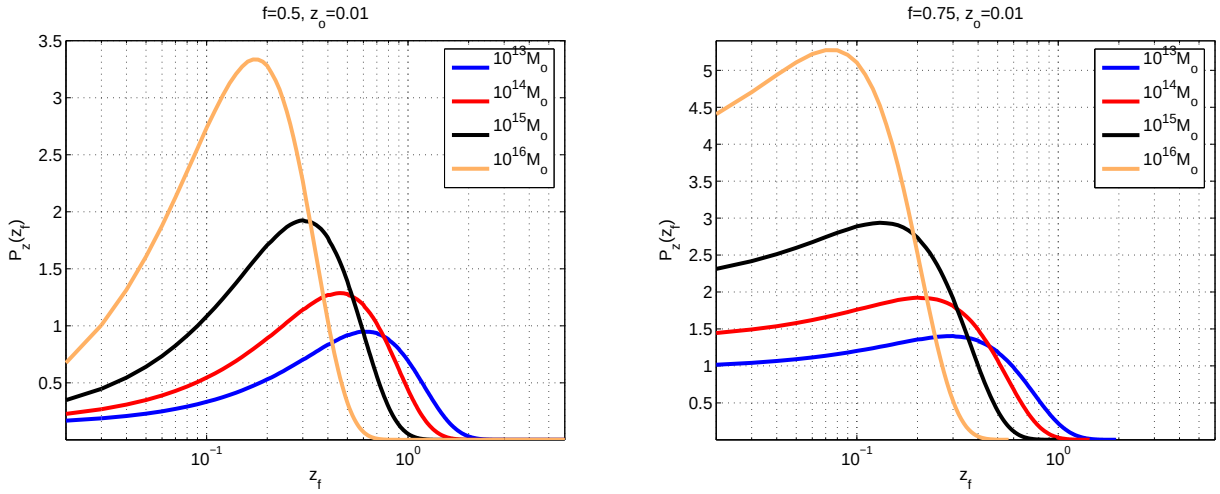

Figure 1. PDF of formation times for the standard ΛCDM model. The blue, red, black and orange curves correspond to halo masses of $10^{13}\ M_\odot$, $10^{14}\ M_\odot$, $10^{15}\ M_\odot$, and $10^{16}\ M_\odot$, respectively, observed at redshift $z_{obs} = 0.01$. The left- and right-hand panels correspond to a mass fraction of $f = 0.5$ and $f = 0.75$, respectively.

mass, or the CPDF of finding a concentration higher than a given value. Such an expression has been deduced (Wechsler et al. 2002) from a statistical sample of haloes identified in N-body simulations,

$$c_v = c_1 a_o / a_c, \tag{5}$$

where $c_1 = 4.1$, and a_o, a_c are the scale factors at the time of observation and formation, respectively, a relation which (according to Wechsler et al.) fits well in the entire mass range explored in their simulations. Note that these authors have defined the characteristic formation time as the epoch in which the mass accretion rate falls below some specified value. This differs from the formation time definition in the LC formalism, where it is defined as the time at which a constant fraction f of the halo mass has been accumulated. To assess the impact of the different definition of the formation time, Wechsler et al. repeated the analysis for merger trees produced by the ESF and compared the resulting halo distribution as function of the formation epoch a_c. Their results suggest that the ESF formalism predicts formation times higher (i.e. later) by a factor 1.25. Therefore, in order to use the scaling described in equation (5) we should first divide the the ESF-based formation times indicated by this factor:

$$a_c = \frac{a_c^{EPS}}{1.25} = \frac{a_{obs}}{1.25(1+z_f)}, \tag{6}$$

where z_f is the formation redshift. Using relation (5) we finally obtain

$$c_v = 5.125 \frac{1+z_f}{1+z_{obs}}, \tag{7}$$

where $a_{obs} \equiv a_0/(1+z_{obs})$. A PDF of the halo concentration parameter can now be derived by using the usual probability distribution transformation law, $P(z_f)\,dz_f = P(c_v)\,dc_v$, such that

$$P(c_v) = P(z_f)\left|\frac{dz_f}{dc_v}\right| = \frac{1+z_{obs}}{5.125} P(z_f), \tag{8}$$

whereas the corresponding CPDF - i.e. the probability that a halo has a concentration parameter higher than a given value - is calculated as $\int_{c_v}^{\infty} P(c'_v)\,dc'_v$.

3 RESULTS

PDF of formation times of haloes with various masses at (observation) redshift $z_{obs} = 0.01$ were calculated using equation (3), and are illustrated in Fig. (1). Haloes were defined to have formed once they assembled a fraction of either $f = 0.5$ (left-hand panel), or $f = 0.75$ (right-hand panel) of their current masses. In both panels of Fig. (1) blue, red, black and orange curves correspond to mass scales of $10^{13}, 10^{14}, 10^{15}$, and $10^{16}\ M_\odot$, respectively. The merger picture describes the formation of haloes as an ongoing process of mutual collapse of subhaloes. Since low-mass subhaloes are more abundant than high-mass subhaloes, haloes of lower masses are more likely to form at higher redshifts. These gradually merge with other subhaloes to form increasingly larger structures, as can be clearly seen in Fig. (1), where low-mass haloes ($10^{13} M_\odot$) form relatively

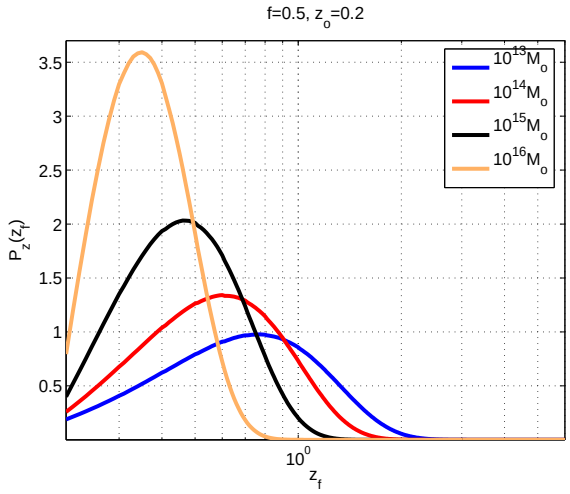

Figure 2. The same as in Fig. (1), but for an observation redshift of $z = 0.2$. (Results shown are only for $f = 0.5$.)

early and at high abundances. The enhancement of the formation time probability and the consequent higher abundances. of subhaloes of this mass scale, imply higher likelihood for a merger to occur and higher-mass objects to form. The latter become progressively more common, and their active formation time - defined as the epoch at which the formation time PDF attains a maximum - peaks at a lower redshift with respect to the active formation epoch of their progenitors.

High abundance of the lowest-mass subhaloes enhances the merger probabilities; as a result these subhaloes grow less common with time. Consequently, the PDF of their formation time is reduced with decreasing redshift, and is eventually dominated by the PDF of their higher-mass products. The process goes on, with ever-increasing mass objects becoming more abundant, accompanied by a reduction of the PDF for lower-mass haloes. This is apparent in either left-hand panel of the figure, where the PDF of formation times peak at lower redshifts with increasing mass. The fall of the curves from the active formation time towards lower redshifts can thus be explained by the fact that low-mass subhaloes hierarchically merge to yield higher-mass subhaloes, thereby diminishing the probability of low-mass objects to form at low redshifts. The corresponding progression in the high-mass halo range can be attributed to the fact that merger rates are substantially reduced with increasing mass. This, too, is in accord with expectations from the ESF, as was demonstrated by, e.g., LC.

The earlier formation times implied by the $f = 0.5$ case with respect to the $f = 0.75$ case are clearly reflected in the plots; the active formation time lies at manifestly higher redshifts in the $f = 0.5$ case. Whereas it peaks at approximately $z = 0.30, 0.20, 0.13, 0.07$ for haloes of $10^{13}, 10^{14}, 10^{15}, 10^{16}\ M_\odot$ for $f = 0.75$, the corresponding formation times with $f = 0.5$ are $z = 0.60, 0.46, 0.30, 0.17$, i.e., at least twice as high. It can also be seen that the PDFs for the $f = 0.5$ case have more pronounced peaks and fall more steeply on either side of the peak than for $f = 0.75$, where the curves are decidedly flatter at lower redshifts than for $f = 0.5$. This clearly is due to the fact that haloes can assemble half of their present mass at considerably earlier stages of their evolution than it takes to assemble 3/4 of their present mass. Thus, their formation times peak at higher redshifts, and the likelihood of merging and forming subhaloes of higher masses increases at higher redshifts as well, resulting in lower probabilities for low-mass haloes to form at low redshifts. We have repeated the calculations for an observation redshift of $z_{obs} = 0.2$ and $f = 0.5$, results for which are illustrated in Fig. (2). Obviously, the PDFs shift to the right, towards higher redshifts, but retain their general shape.

Results of the PDF and CDPF of halo concentrations are presented in Fig. (3) for observation redshifts of $z_{obs} = 0.01$ and $z_{obs} = 0.2$. For $z_{obs} = 0.01$, haloes with 10^{13}, 10^{14}, 10^{15}, $10^{16}\ M_\odot$ peak at concentrations $c_v \sim 8.1, 7.4, 6.6, 6.0$, respectively. The corresponding peak concentrations for $z_{obs} = 0.2$ are $c_v \sim 7.6, 7.2, 6.2, 5.8$, i.e. somewhat lower, since the higher observation redshift limits the redshift range available for halo formation. The CPDFs plotted in the right-hand panels of Fig. (3) provide a convenient means of determining the probability of finding a concentration higher than a given value. For example, at $z_{obs} = 0.01$ the probability of finding haloes of 10^{13}, 10^{14}, 10^{15}, $10^{16}\ M_\odot$ with concentrations higher than $c_v = 10$ are $\sim 0.29, 0.11, 0.007, 2.2 \cdot 10^{-7}$. For $z_{obs} = 0.2$ the corresponding values are $\sim 0.16, 0.03, 4.4 \cdot 10^{-4}, 4.0 \cdot 10^{-11}$. Clearly, the probability for a high value of c_v in a $\sim 10^{15} M_\odot$ cluster is quite low in the standard ΛCDM cosmology.

4 THE CASE OF A1689

Recently, Broadhurst & Barkanna (2007, hereafter BB) have reported the results of a comparative study of Einstein radii calculated for a large sample of simulated clusters of masses $\sim 10^{15}\ M_\odot$, and those observed in the three massive clusters A1689, C10024-17, and A1703. While the simulations yield Einstein radii in the range $\sim 15 - 25$", the measured values for

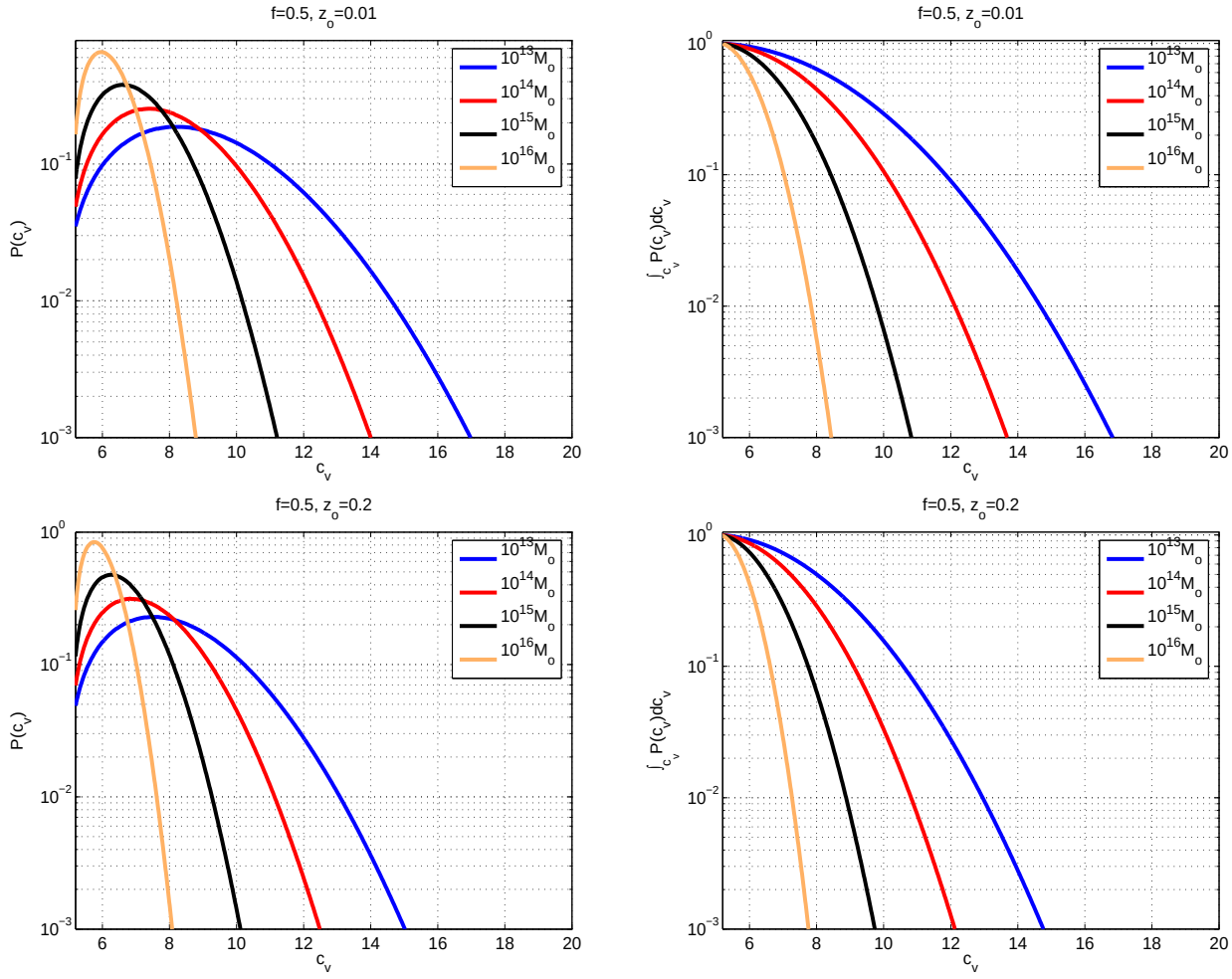

Figure 3. The PDF (left) and CPDF (right) of the halo concentration parameter. Upper and lower panels correspond to observation redshifts of 0.01 and 0.2, respectively.

these clusters are $\sim 50", 31"$, and $32"$, respectively, a result which is seen by BB to constitute a challenge to the standard ΛCDM model.

Since we know all relevant properties of A1689, namely its virial mass, virial radius, concentration parameter (assuming an NFW DM profile), redshift, and the lensed source redshift, it is possible to construct a PDF of Einstein radii for an A1689-like cluster. The equation governing the relation between the concentration parameter and the Einstein radius is, assuming an NFW profile (BB),

$$\left(\frac{4R_v\rho_c^z\Delta_c}{3\Sigma_{cr}}\right)\frac{c_v^2}{\ln(1+c_v)-c_v/(1+c_v)}\frac{g(x)}{x^2}=1, \tag{9}$$

where R_v, ρ_c^z, Δ_c, and Σ_{cr} are the virial radius, critical density at redshift z, overdensity at virialisation, and critical surface density, respectively. All these quantities are specified by BB, with the exception of the virial radius, for which we adopt the theoretical value found from the relation $M_v=\frac{4\pi}{3}\rho_c(z)\Delta_c(z)R_v^3$, resulting in $R_v=2.63\,Mpc$, for $h=0.687$. Also, $x\equiv\frac{R_E c_v}{R_v}$, where R_E is the Einstein radius, and

$$g(x)=\ln\frac{x}{2}+\begin{cases}1, & x=1\\ \frac{2}{\sqrt{x^2-1}}\tan^{-1}\sqrt{\frac{x-1}{x+1}}, & x>1\\ \frac{2}{\sqrt{1-x^2}}\tanh^{-1}\sqrt{\frac{1-x}{1+x}}, & x<1\end{cases}. \tag{10}$$

The solution of Eq. (9) provides the Einstein radius as a function of c_v, from which it is trivial to derive the angular Einstein radius, $\theta_E = R_E/D_A(z_l)$, the ratio between the (physical) Einstein radius and the angular diameter distance to the lens, the measured redshift of A1689, $z_l = 0.183$. It remains to determine the PDF of the angular Einstein radius. This can be accomplished using once more the transformation law of probability distribution functions:

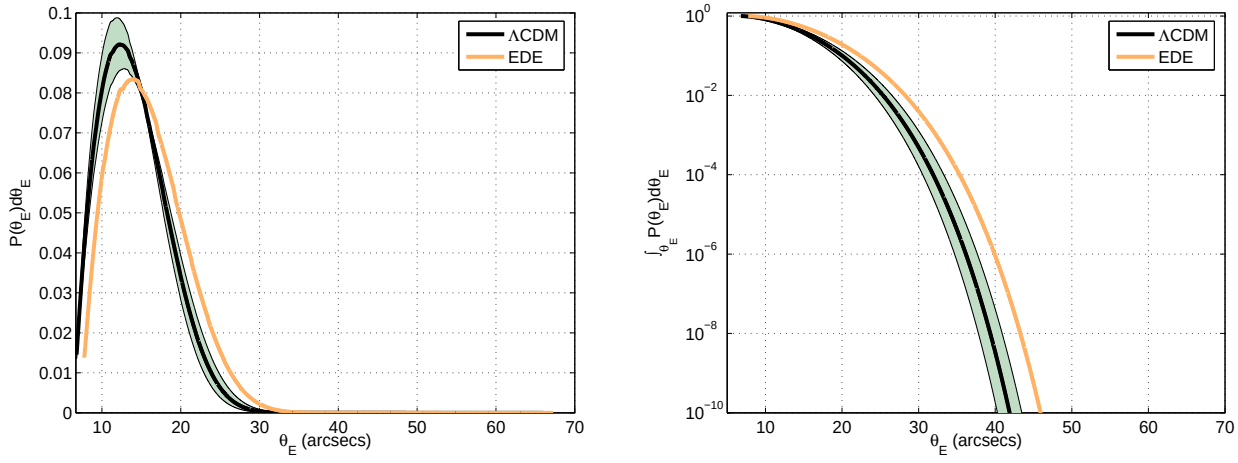

Figure 4. The PDF (left) and CPDF (right) of the Einstein radius for an A1689-like cluster. Continuous black and orange curves correspond to the standard ΛCDM and EDE models, respectively. The shaded areas reflect the variance generated by incorporating the 2σ uncertainty in the cosmological parameters h, n, and σ_8 in the calculations for the ΛCDM model.

$$P(\theta_E)d\theta_E = P(c_v)dc_v = P(z_f)dz_f, \tag{11}$$

from which we obtain

$$P(\theta_E) = P(c_v)\left|\frac{dc_v}{d\theta_E}\right| = P(z_f)\left|\frac{dz_f}{dc_v}\right|\left|\frac{dc_v}{d\theta_E}\right|. \tag{12}$$

The first derivative is calculated analytically using Eq. (7), whereas a numerical calculation based on the $\theta_E(c_v)$ relation in Eq. (9) is used in order to infer the second derivative.

Results for the PDF and CDF of the angular Einstein radius for an A1689-like cluster are presented in Fig. (4). The results generated within the framework of the standard ΛCDM are represented by the black continuous curve; the shaded areas represent the 2σ uncertainties in the cosmological parameters Ω_m, n, and σ_8. As is clear from the figure, large Einstein radii ($\gtrsim 40$") have extremely low probabilities in the standard ΛCDM universe. In fact, the cumulative probability for an A1689-like cluster to induce an angular Einstein radius larger than 40" amounts to $\sim 3.4\cdot 10^{-9}$ in this model; the corresponding probability for the $+2\sigma$ level increases to $\sim 4.1\cdot 10^{-8}$.

Non-standard cosmological models characterised by earlier evolution of the large scale structure may resolve the apparent discrepancy between measured and predicted values of R_E, by virtue of earlier halo formation times, reflected in higher central halo concentrations and, therefore, higher probabilities for large Einstein radii. For example, models based on positively skewed primordial density fluctuations lead to earlier growth of the large scale structure. Early dark energy (hereafter EDE) models provide another alternative for inducing earlier formation times by virtue of the modified cosmic dynamics implied by a non-negligible DE component in the early universe. To explore this possibility, we have repeated our calculations for a specific EDE model, with an early quintessence density parameter $\Omega_d^e = 0.03$ and equation of state coefficient $w_0 = -0.9$ at $z = 0$. These parameters are consistent with recent WMAP results (Doran & Robbers, 2006). The other cosmological parameters were not modified, with the exception of $\sigma_8 = 0.51$, a value obtained by normalizing the cumulative halo mass function to the same number of halos generated in the standard ΛCDM model. Complete details concerning the calculation of the relevant large scale quantities within the framework of EDE models can be found in, e.g., Bartelmann, Doran, & Wetterich (2006) and Sadeh, Rephaeli & Silk (2007). The latter work was motivated by the possible need to have a higher level of CMB anisotropy induced by the Sunyaev-Zeldovich effect than is predicted in the standard ΛCDM model.

Results of the PDF and CDF of the Einstein radius for A1698 are shown by the continuous orange curve of Fig. (4). Note that for the EDE model the theoretically inferred virial radius reduces slightly to $r_v = 2.54\,Mpc$. The probability for an A1689-like cluster to produce an Einstein radius larger than 40" in this model is $\sim 9.1\cdot 10^{-7}$, i.e., approximately two orders of magnitude higher than the corresponding probability in the ΛCDM model. The $+2\sigma$ uncertainty (which is not shown in the plot) in the cosmological parameters would lead to even higher probabilities than those indicated by the orange curve of the EDE model. However, these probabilities are still very low.

5 DISCUSSION

The observationally inferred high concentration parameters associated with several massive clusters have been claimed to constitute a major challenge to the currently favoured standard cosmological model. Such high concentrations are expected in haloes formed at relatively high redshifts, reflecting the high universal background density at that time. As Einstein radii in lensing haloes increase monotonically with their concentration parameters, observed high radii also indicate earlier formation times. Massive clusters form preferentially at low redshifts, as attested by results of both N-body simulations and semi-analytic calculations based on the excursion set theory.

Our assessment of the apparent discrepancy between theoretical predictions and measurements of the concentration parameter and Einstein radii of high-mass clusters has been based on the assumption of NFW mass profiles. This is motivated by the explicit use of this profile in the analysis of N-body simulations (Wechsler et al. 2002, Neto et al. 2007), which were used to derive the scaling relation between c_v and t_f equation (7) in these works, and had to be adopted in our analysis for consistency. The NFW profile is not the only profile that provides an acceptable fit to simulated haloes. It is quite possible that most of the discrepancy explored here stems from the insistence on using the NFW profile. Even so, the fact that this profile is used extensively in the description of galaxies and clusters provides sufficient motivation to focus on its implications in the context of our work here.

If indeed the apparent discrepancy is considered a serious difficulty for the standard model, then it is only reasonable to consider close alternatives to the standard ΛCDM model. Earlier formation times are naturally predicted in non-standard cosmologies, such as those characterised by non-Gaussian, positively skewed primordial density fluctuations, and early dark energy models. We have shown in this work that cosmological models incorporating an early DE component may induce higher probabilities of finding large Einstein radii in A1689 than in the standard ΛCDM model, although perhaps not sufficiently high to remove the apparent conflict between theory and observations.

The calculation of the number of clusters whose masses and redshifts are comparable to or larger than those of A1689, and which are expected to induce Einstein radii larger than a given value, is not simple since this would require an integration over the formation time PDFs of all of these masses and redshifts. In addition to this technical issue, one would also need to draw an arbitrary source redshift so as to be able to calculate the corresponding angular diameter distances needed in Eq. (9). However, we can provide a crude estimate of the upper limit to this number by integrating the relevant PS mass functions - shown in Fig. (6) for both models at observation redshifts $z_{obs} = 0.01$ and $z_{obs} = 3$ - over the mass range $[10^{15}\, M_\odot, \infty]$.

With our specific choice of cosmological parameters, the standard ΛCDM and EDE models described in this work predict ~ 50 (~ 157 for the $+2\sigma$ level of σ_8 - which agrees better with the corresponding figure inferred from large scale studies), and ~ 300 cumulative cluster counts with $M \geqslant 10^{15}\, M_\odot$ and $z_{obs} \geqslant 0.183$, respectively. Obviously, not all of these clusters have Einstein radii larger than 40", as these depend also on the redshifts of the lensed objects. We can readily set an upper limit on the number of clusters with $\theta_E \geqslant 40$", whose mass and redshift are within these ranges, by multiplying the cumulative numbers by the probabilities of finding an A1689-like cluster with $\theta_E \geqslant 40$". As specified in the previous section, these probabilities are $3.4 \cdot 10^{-9}$ (or $4.1 \cdot 10^{-8}$ at the $+2\sigma$ level), and $9.1 \cdot 10^{-7}$ in the standard ΛCDM and EDE models, respectively. Thus, the estimated numbers of clusters are $\sim 1.7 \cdot 10^{-7}$ ($6.4 \cdot 10^{-6}$ at the $+2\sigma$ level) and $\sim 2.7 \cdot 10^{-4}$ in the ΛCDM and EDE models, respectively.

It is important to realize that while our analysis of the PDF of the concentration parameter and Einstein radius poses an appreciable difficulty for the standard large scale model, it cannot be construed as insurmountable evidence against the validity of the standard ΛCDM model. In fact, there is a significant level of uncertainty in the relation between the formation time and concentration parameter, an uncertainty which we have not yet taken explicitly into account. Many factors contribute to this uncertainty, including the reported variance in the scaling, as shown by Wechsler et al. to be at the level of $\sim 50\%$, such that, for example, a halo with mass $10^{14} M_\odot h^{-1}$ would have a concentration $c_v \sim 7 \pm 3$, representing only the 1σ uncertainty level. The actual uncertainty may even be appreciably higher, due to the fact that the baryonic component was ignored in the cited N-body simulations, and due to the large degree or arbitrariness in the definition of the formation time.

The higher than predicted value of θ_E is reflected more directly in the discrepancy between the theoretically predicted and measured values of R_v. The solutions of Eq. (9), which yield the Einstein radius as a function of concentration parameter, are very sensitive to the virial radius of the cluster. We have used the most probable theoretically-inferred values of R_v in our calculations, $R_v = 2.63$ and $2.55\, Mpc$ in the standard ΛCDM and EDE models, respectively. But these values too could be uncertain; we explore here the impact of a variance of $\sim 20\%$ in R_v that would presumably reflect the intricacies of the process of hierarchical clustering through mergers and non-spherical collapse, which was shown (e.g. Del Popolo 2002) to yield significantly lower virialisation overdensities than predicted in the spherical collapse scenario. For example, an isolated prolate spheroid of axial ratio $a_3/a_1 = 2.4 : 1$, which is the mean ratio found in an N-body simulation in which 878 clusters were identified (Hennawi et al. 2007), was shown by Del Popolo to have a virialisation overdensity of $\Delta_c \sim 50$, lower by more than a factor 3 than the corresponding quantity for a spehrical virialised region. (Although carried out in the context of an Einstein de Sitter universe, the reported results are not likely to change qualitatively in a ΛCDM model.) For a given mass and redshift, $M_v = \frac{4\pi}{3} \rho_c(z) \Delta_c(z) R_v^3$, the lower overdensities obviously imply larger virial radii.

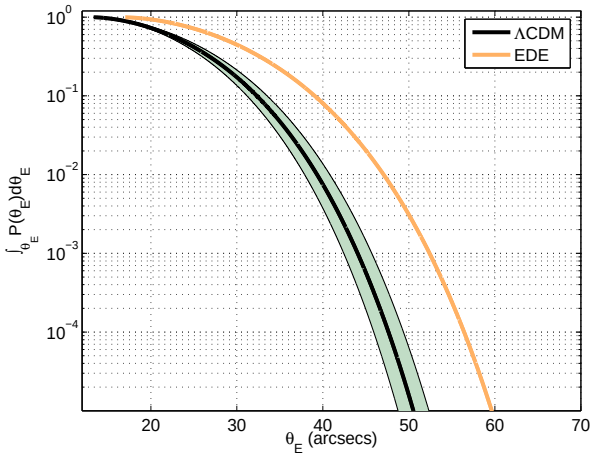

Figure 5. The same as Fig. (4), but for $R_v = 3.1\,Mpc$.

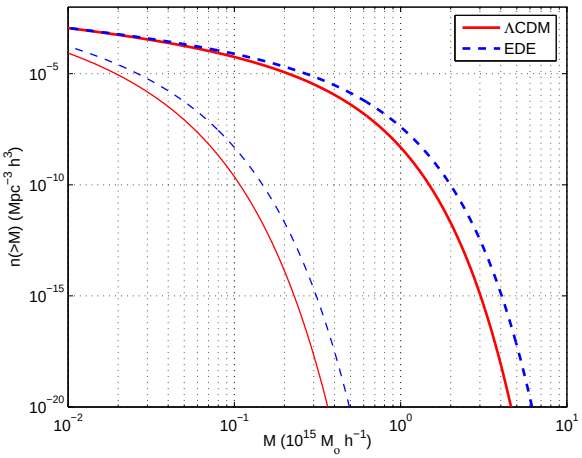

Figure 6. The cumulative PS mass functions for the standard ΛCDM (red continuous curve) and EDE (blue dashed curve) models. Thick and thin lines correspond to observation redshift $z_{obs} = 0.01$ and $z_{obs} = 3$, respectively.

A larger virial radius is also in accord with the results of a recent detailed, model-independent analysis of A1689 by Lemze et al. (2008), who (deduced the mass profile and) determined $R_v = 2.14\,Mpc \cdot h^{-1}$ from joint fitting to extensive X-ray and lensing measurements. With $h = 0.687$ we have $R_v = 3.1\,Mpc$, which is indeed higher by $\sim 20\%$ than the theoretically predicted value for this cluster. This has a very significant impact on the PDF and CPDF of the Einstein radius, as demonstrated in Fig. (5).

With this larger virial radius, the probability for an A1689-like cluster to have $\theta_E \geqslant 40$" is $8 \cdot 10^{-3}$ (or $1.3 \cdot 10^{-2}$ at the $+2\sigma$ level) in the standard ΛCDM model, and $8 \cdot 10^{-2}$ in the EDE model. These large differences originate in the larger Einstein radii predicted by Eq. (9) for the same concentration parameter, and give rise to substantially higher upper limits on the number of clusters expected to be detected with $\theta_E \geqslant 40$", ~ 1.3 (at the $+2\sigma$ level), and as many as ~ 24 in the standard ΛCDM and EDE models, respectively.

Finally, we note that the above considerations indicating significantly higher halo concentrations and larger Einstein radii in clusters may have significant ramifications for the non-standard, EDE model: Had the simulations been carried out within the framework of a specific EDE model, the formation time - concentration scaling would have probably predicted higher concentrations, by virtue of the earlier formation of structure. Here, too, the probabilities of finding haloes with high concentrations and Einstein radii would be markedly higher, perhaps even prohibitively higher, so much so that this could turn out to be a significant constraint on the parameters of this model.

6 ACKNOWLEDGMENT

Useful discussions with Dr. Tom Broadhurst are gratefully acknowledged. This work was supported by a grant from the Israel Science Foundation.

7 REFERENCES

Bartelmann M., Doran M., Wetterich C., 2006, *Astron. Astrophys.* , 454, 27
Bond J.R., Cole S., Efstathiou G., & Kaiser N., 1991, *ApJ* , 379, 440
Broadhurst T.J., Barkanna R., 2008, preprint (astro-ph/0801.1875)
Bullock J.S., Kolatt T.S., Sigad Y., Somerville R.S., Kravtsov A.V., Klypin A.A., Primack J.R., Dekel A., 2001, *MNRAS* , 321, 559
Del Popoplo A., 2002, *Astron. Astrophys.* , 387, 759
Doran M., Robbers G., 2006, *J. Cosmo. Astro. Phys.* , 6, 26
Jing Y.P., 2000, 535, 30
Lacey C., Cole S., 1993, *MNRAS* , 262, 627
Lemze D., Barkana R., Broadhurst T.J., Rephaeli Y., 2007, preprint (astro-ph/0711.3908)
Navarro J.F., Frenk C.A., & White S.D.M, 1995, *MNRAS* , 275, 720
Neto A.F., Gao L., Bett P., Cole S., Navarro J., Frenk C.S., White S.D.M, Springel V., Jenkins A., 2007, *MNRAS* , 381, 1450
Press W.H. & Schechter P., 1974, *ApJ* , 187, 425
Sadeh S., Rephaei Y., Silk J., 2007, *MNRAS* , 380, 637
Spergel D.N. et al. 2007, *Ap. J. Supp.* , 170, 377
Wechsler R.H., Bullock J.S., Primack J.R., Kravtsov A.V., & Dekel A., 2002, *ApJ* , 568, 52
Zhao D.H., Mo H.J., Ping Y.P., & Börner G., 2003, *MNRAS* , 339, 12

This paper has been typeset from a TEX/ LATEX file prepared by the author.